Modeling and Rendering Glow Discharge

VENKATARAM SIVARAM, University of California San Diego, USA
RAVI RAMAMOORTHI, University of California San Diego, USA
TZU-MAO LI, University of California San Diego, USA

Fig. 1. **Rendering glow discharge.** This work presents a model for the emission from glow discharge, a visible electrical discharge commonly seen in Neon lights. We derive a set of physically based equations that enable efficient estimation of the emitted frequencies. Our emission model integrates seamlessly with existing volume rendering architectures and participates naturally in light transport effects. The **Chess** scene above is lit entirely through instances of glow discharge. Scene adapted from Chess Set Model by Riley Queen ©Poly Haven.

Previous research in material models for surface and volume scattering has enabled highly realistic scenes in modern rendering systems. However, there has been comparatively little study of light sources in computer graphics despite their critical importance in illuminating and bringing life into these scenes. In the real world, photons are emitted through numerous physical processes including combustion, incandescence, and fluorescence. The qualities of light produced in each of these processes are unique to their physics, making them interesting to study individually.

In this work, we propose a model for glow discharge, a form of light-emitting electrostatic discharge commonly found in Neon lights and gas discharge lamps. We take inspiration from works in computational physics and develop an efficient point-wise solver for the emission due to glow discharge suitable for traditional volume rendering systems. Our model distills the complex mechanics of this process into a set of flexible and interpretable parameters. We demonstrate that our model can replicate the visual qualities of glow discharge under varying gases.

CCS Concepts: • **Computing methodologies** → **Volumetric models**; **Ray tracing**.

ACM Reference Format:
Venkataram Sivaram, Ravi Ramamoorthi, and Tzu-Mao Li. 2025. Modeling and Rendering Glow Discharge. In *Special Interest Group on Computer Graphics and Interactive Techniques Conference Conference Papers (SIGGRAPH Conference Papers '25), August 10–14, 2025, Vancouver, BC, Canada.* ACM, New York, NY, USA, 11 pages. https://doi.org/10.1145/3721238.3730674

1 Introduction

Along with complex materials and surface details, realistic lighting models are a crucial component of scene design in modern computer graphics. Despite this, the amount of work in accurately modeling light sources is scarce relative to material and surface modeling. In part, this is due to the adequacy of existing light source primitives, such as area, spot, and directional lights as well as heterogeneous volumes in more extreme cases. While this approach to scene lighting is productive, it becomes difficult to design lighting to mimic more complex phenomena such as lightning, Aurora Borealis, fluorescence, and more. The challenge in these cases is the sophisticated

Authors' Contact Information: Venkataram Sivaram, ves223@ucsd.edu, University of California San Diego, USA; Ravi Ramamoorthi, ravir@cs.ucsd.edu, University of California San Diego, USA; Tzu-Mao Li, tzli@ucsd.edu, University of California San Diego, USA.

SIGGRAPH Conference Papers '25, Vancouver, BC, Canada

ACM ISBN 979-8-4007-1540-2/2025/08
https://doi.org/10.1145/3721238.3730674

physical processes that govern the corresponding visual effects. It is challenging to approximate these processes using existing primitives. We are motivated by this limitation and aim to tackle unique emissive phenomena from their physics-based foundations.

In this work, we present a model for glow discharge that simulates the dynamics of subatomic and molecular particle densities that arise from this specific kind of electrical discharge. The primitives in our model can be constructed from a set of coefficients describing the properties of these dynamics and a vector field indicating the general flow of electrons. We then estimate the point-wise emissions due to glow discharge by solving for the particle densities using modified equations that describe the fundamental physics. Additionally, we incorporate the ambient gas' spectroscopic properties into the emission calculations. This allows us to replicate the visual qualities of glow discharge observed in various gases. Our point-wise emission formulation is a natural component of the volumetric rendering equation and can be easily incorporated into volume rendering algorithms.

Although our model is physically based, it does not sacrifice flexibility. It is parameterized by a drift velocity field (Section 4.2) with a high degree of freedom, which enables our model to simulate the glow discharge of interesting shapes, as shown in Figure 1. We also describe how to use Bezier curves as primitives for modeling the visual qualities of glow discharge found in the real world (Section 5.3).

Our contributions are summarized as follows:

- A set of equations (Section 4.2) which efficiently models the growth of electrons and positive and negative ions in glow discharge following its physical processes (Section 3).
- A numerical algorithm to solve for the number densities of charged particles (Sections 4.3, 4.4) and calculate the corresponding spectroscopic emissions (Section 5.1).
- A representation to visually model common forms of glow discharge and perform volume rendering with (Section 5).

2 Background and Previous Work

Our work builds on volume rendering in computer graphics, and the physical foundations of electrostatic discharge, lightning, streamer propagation and flames. We refer readers to Table 1 for an overview of the notation used throughout the rest of this paper.

Volume rendering. The governing principles of volumetric light transport are typically described by the *equation of transfer* [Chandrasekhar 1960; Pharr et al. 2016] along rays $\boldsymbol{x} = \boldsymbol{x}_0 + t\boldsymbol{\omega}$ as follows:

$$\frac{\partial L_\mathrm{o}(\boldsymbol{x}, \boldsymbol{\omega})}{\partial t} = L_\mathrm{e}(\boldsymbol{x}, \boldsymbol{\omega}) + L_\mathrm{s}(\boldsymbol{x}, \boldsymbol{\omega}) - \sigma_\mathrm{t}(\boldsymbol{x}, \boldsymbol{\omega}) \cdot L_\mathrm{i}(\boldsymbol{x}, -\boldsymbol{\omega}), \quad (1)$$

Above, $L_\mathrm{e}(\boldsymbol{x}, \boldsymbol{\omega})$ accounts for the emission of the medium, $L_\mathrm{s}(\boldsymbol{x}, \boldsymbol{\omega})$ and $L_\mathrm{i}(\boldsymbol{x}, \boldsymbol{\omega})$ model the in-scattered light and absorption, and the coefficients σ_t and σ_s are related to the extinction and scattering of radiance. In this work, we are concerned with the emission term $L_\mathrm{e}(\boldsymbol{x}, \boldsymbol{\omega})$, and we treat glow discharge as a purely emissive volume, meaning that $\sigma_\mathrm{s} = \sigma_\mathrm{t} = 0$. As such, Equation 1 becomes

$$L_\mathrm{o}(\boldsymbol{x}_0, \boldsymbol{\omega}, \lambda) = \int_0^d L_\mathrm{e}(\boldsymbol{x}, \boldsymbol{\omega}, \lambda)\, dt, \quad (2)$$

where $\boldsymbol{x}_0$ is the ray origin, $\boldsymbol{x}$ is the ray $\boldsymbol{x}_0 + t\boldsymbol{\omega}$, d is the distance along $\boldsymbol{\omega}$ to a surface interaction or the end of the volume, and λ is the wavelength. Typically, the emission term is prescribed by a discrete volume database generated from offline computations, for example, by performing a global solve of the dynamics of a physical process to obtain light quantities and caching the results in a dense grid. Our goal instead is to estimate this emission at arbitrary points $\boldsymbol{x}$ without prior computation.

Table 1. **Notation.** Table of notation used throughout this paper.

Symbol(s)	Meaning
$\boldsymbol{x}$	Arbitrary point in space, $\mathbb{R}^3$
$\boldsymbol{\omega}$	Outgoing radiance direction, $\mathbb{S}^2$
$L_\mathrm{o}(\boldsymbol{x}, \boldsymbol{\omega})$	Outgoing radiance from $\boldsymbol{x}$ along $\boldsymbol{\omega}$
$L_\mathrm{e}(\boldsymbol{\omega}, \boldsymbol{\omega})$	Emission at $\boldsymbol{x}$ along $\boldsymbol{\omega}$
$E, \widetilde{E}$	Electron number density, logarithm
$P, \widetilde{P}$	Positive ion number density, logarithm
$N, \widetilde{N}$	Negative ion number density, logarithm
$\vec{v}_E, \vec{v}_P, \vec{v}_N$	Drift velocity of electrons and ions
$\mathcal{D}$	Diffusion coefficient
α	Ionization coefficient
β	Recombination coefficient
η	Attachment coefficient
ρ	Ion scale coefficient
$\vec{\mu}$	Homogenized drift velocity, $\mathbb{R}^3$
λ	Wavelength of light

Electrical discharge. Under normal circumstances, electrons flow through conducting materials such as metal electrodes. However, when there exists sufficient electric field strength in an area, it can cause a *dielectric breakdown*, where the dielectric medium between electrodes becomes ionized [Massines et al. 1998]. In such a state, the medium acts as a conductor, permitting the flow of charge. This is referred to as electrical discharge, which comes in many forms depending on the voltage, current, and the medium. Notable examples of electrical discharges are lightning, spark discharge, and glow discharge. Glow discharge, also known as a type of plasma, is formed by passing an electric current through a gas, typically at low pressures [Winchester and Payling 2004]. It is distinct from corona discharge, which occurs at atmospheric pressure, and Saint Elmo's fire, which is a specific manifestation of corona discharge. Glow discharges are characterized by their luminosity, which is produced when electrons gain sufficient energy to excite gas molecules, resulting in the emission of photons. Our work focuses on glow discharges as they are more controlled in scale and temporally coherent compared to other electrical discharge phenomena.

Simulating lightning. Lightning is an appealing natural phenomenon that has caught the attention of many previous works [Betz et al. 2008; Cooray 2015; Dwyer and Uman 2014]. Although it appears as a collection of randomly connected segments, scientific experiments reveal some structure in lightning formation. For example, it is now known that lightning strikes begin with a stepped leader descending from clouds towards the ground [Rizk 2024], after which an immense channel current called the return stroke is

released, producing the strong visible emissions we perceive as lightning [Cruz et al. 2025]. During this process, several other strands of ionized air, called streamers, may form both from the ground and the cloud, contributing to the formation of the main lightning channel [Malagón-Romero and Luque 2019]. In computer graphics, previous works have focused on modeling these aspects of lightning [Reed and Wyvill 1994; Sosorbaram et al. 2001] by using pseudo-random numbers or a probabilistic model. However, to our knowledge, no work in computer graphics has modeled the physical processes underlying this phenomenon in conjunction with applications in light transport. Our work bridges the gap between physical theory and computational practice. While we do not explicitly attempt to simulate lightning, our methodology can extend beyond small-scale phenomena such as glow discharge.

Streamer propagation. Previous works in the physics domain have explored semi-empirical methods for studying the formation of glow discharge. We are primarily interested in the work of Morrow and Lowke [1997] and Georghiou et al. [2000], which models the evolution of the number densities of electrons and gas ions. We discuss the equations presented in these works in Section 3.3 (see Equations 3), and how they relate to our application and the physical processes of glow discharge.

Previous work in the physics literature [Georghiou et al. 2000] has used finite element methods (FEM) to solve these equations for fixed boundary conditions in two dimensions. This approach is orthogonal to our desired goal of evaluating point-wise emissions due to these dynamics, irrespective of the time domain and while retaining flexible boundary conditions. Therefore, while we take inspiration from these equations in our model, we address significant computational challenges by simplifying certain terms to enable efficient evaluation of point-wise emission.

Flames. Similarly to glow discharge, flames are light-emitting phenomena with interesting underlying physical processes. In the past, extensive work has been done to simulate the thermodynamical evolution of combustion [Nielsen et al. 2022]. The translation from volumetric databases of combustion to light transport simulation was accomplished by [Pegoraro and Parker 2006]. This work carefully considers the scattering, radiative, refractive, and emissive properties to construct a complete volume rendering solution to visualize flames. We take inspiration from their work as the foundation we use for the spectral emission of glow discharge relies on similar mechanics to those found when modeling flames.

3 Glow Discharge Process

This section lays the scientific foundation for studying glow discharge. Additionally, we relate the physics involved to concrete mathematical models used in Equation 3.

3.1 Overview

Glow discharge is a nonthermal and nonequilibrium plasma which is primarily influenced by electric fields. As such, it does not fall under the typical regime of thermal plasmas assumed in magnetohydrodynamics. Under strong electric fields, free electrons generated by background radiation (e.g. cosmic rays) are accelerated to high kinetic energies, enabling them to cause electron-impact ionization events. These ionization events generate new electrons and ions that partake in a similar process, ultimately creating a cascading effect. The resulting phenomenon, depicted in the inset below, is referred to as *secondary emission*, *electron avalanche* or *Townsend avalanche* [Flugge 1955; Gewartowski and Watson 1965].

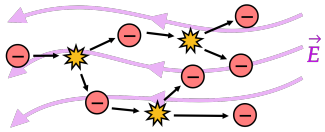

3.2 Collisional Processes

In electron avalanches, some specific processes govern the generation of free particles and emitted photons. We describe them below and, for simplicity, consider diatomic molecular gases of the form X_2 such as Hydrogen (H_2) and Helium (He_2). These interactions are also visualized in Figure 2.

Ionization. When electrons gain sufficient kinetic energy above the binding energy of the outermost electron of X_2, they are increasingly likely to collide with this outermost electron and eject it from its orbit.

$$e^- + X_2 \rightarrow X_2^+ + 2e^-$$

In the process, an additional free electron is generated, along with a positive ion.

Recombination. Occasionally, particles of opposing charges collide with each other and neutralize:

Recombination (Ion-Electron)

$$e^- + X_2^+ \rightarrow X_2 + \gamma$$

Recombination (Ion-Ion)

$$X_2^- + X_2^+ \rightarrow 2X_2 + \gamma$$

In the process, photons (γ) are emitted, though these are typically in the ultraviolet spectrum [Riba 2022] and are not visible to the human eye.

Attachment. With sufficient energy, electrons may instead attach themselves onto molecules of gas:

Attachment

$$e^- + X_2 \rightarrow X_2^-$$

This produces negative ions which subsequently participate in the processes of glow discharge.

Excitation. Even when electrons have insufficient energy for ionization, they may still collide with an electron in orbit. In such cases, the molecule may be elevated to a higher energy level:

Excitation

$$e^- + X_2 \rightarrow X_2^* + e^-$$

De-excitation

$$X_2^* \rightarrow X_2 + \gamma$$

These excited molecules persist only for a short duration, eventually returning to their ground state, during which a photon is released. It is these photons which primarily consistute the visual appearance of glow discharge.

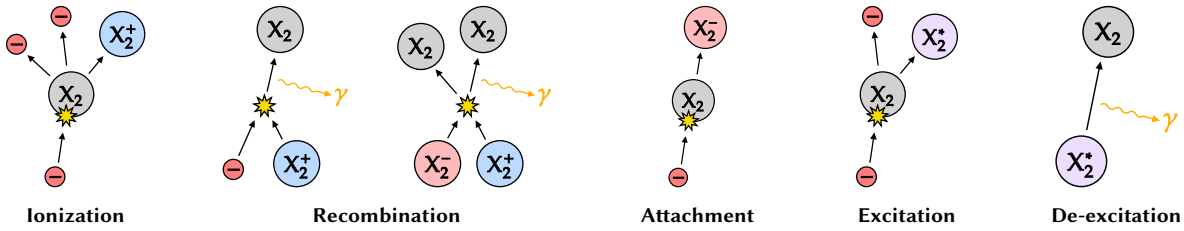

Fig. 2. **Physical processes in glow discharge.** The numerous particles generated from electron avalanches in glow discharge undergo several interesting physical processes as shown above. Processes such as ionization, attachment, and excitation introduce additional particles into the system. On the other hand, recombination and de-excitation consume particles in exchange for light. While electron-ion and ion-ion recombination emits photons, these are typically outside the visible spectrum.

Each of these processes is relevant to our model of glow discharge. Ultimately, for lighting, we care mostly about the amount of excitation and de-excitation, which generates the majority of visible light in glow discharge.

3.3 Mathematical Relations

The physical processes described above have been modeled in prior works in physics [Georghiou et al. 2000; Morrow and Lowke 1997] using the equations below:

$$\frac{\partial E}{\partial t} = \underbrace{\alpha\|\vec{v}_E\|E}_{\text{Ionization}} - \underbrace{\eta\|\vec{v}_E\|E}_{\text{Excitation}} - \underbrace{\beta EP}_{\text{Recombination}} - \underbrace{\nabla\cdot(E\vec{v}_E)}_{\text{Advection}} + \underbrace{\nabla\cdot(\mathcal{D}\nabla E)}_{\text{Diffusion}} \tag{3a}$$

$$\frac{\partial P}{\partial t} = \alpha\|\vec{v}_E\|E - \beta EP - \beta NP - \nabla\cdot(P\vec{v}_P) \tag{3b}$$

$$\frac{\partial N}{\partial t} = \eta\|\vec{v}_E\|E - \beta NP - \nabla\cdot(N\vec{v}_N) \tag{3c}$$

Above, E, P, and N are the number densities of the electrons and positive and negative ions within the system. These densities are influenced by first-order flows by their corresponding drift velocities $\vec{v}_E, \vec{v}_P, \vec{v}_N$. Interdependent and high-order effects arise in proportion to the spatially varying coefficients α, β, η, and $\mathcal{D}$ which account for ionization, recombination, attachment, and diffusion, respectively. In the following, we dissect the terms highlighted above.

Ionization. Equations 3a and 3b include the term $\alpha\|\vec{v}_E\|E$ which accounts for the production of additional particles due to ionization. The parameter α roughly controls the cross-section of ionization.

Recombination. Electron-ion recombination is modeled by the term βEP which is found in Equations 3a and 3c. Similarly, ion-ion recombination is handled by the term βNP in Equations 3b and 3c. The negative sign of the term reflects the fact that the original particles are consumed in the neutralization process. Similar to α, the coefficient β controls the probability that these particles undergo recombination. Intuitively, one can think of β as a drag coefficient that reduces the growth rate of the electrons and ions.

Attachment. The term $\eta\|\vec{v}_E\|E$ is included in Equations 3a and 3c. The opposite signs in these equations are because electrons are consumed in the attachment process and generate negative ions. Here, the coefficient η has the immediate effect of reducing growth attributed to ionization. It also has a second-order effect since the increase in negative ions also impacts the growth of positive ions.

Emission. Morrow and Lowke [1997] and Morrow [1985] suggest to model the intensity of emissions at a point $\boldsymbol{x}$ proportional to $\|\vec{v}_E\|E$. We set the proportionality constant to $\sigma_0 = 0.42 \cdot 10^{-18}$, the collision cross section in air [Atkins and De Paula 2006; Benyoucef and Tahri 2017]. For our purposes, this implies the following:

$$\underbrace{\int_\Lambda L_e(\boldsymbol{x},\boldsymbol{\omega},\lambda)\,d\lambda = \left(\frac{\sigma_0}{4\pi}\right)\|\vec{v}_E\|E(\boldsymbol{x})}_{\text{Emission Strength}} \tag{4}$$

We divide by 4π assuming that this light is emitted isotropically. Intuitively, this expression characterizes the rate of excitation and de-excitation in the same way as ionization. For our end goal of rendering glow discharge, we ultimately want to evaluate $L_e(\boldsymbol{x},\boldsymbol{\omega},\lambda)$, and this requires estimating the number densities of electrons, and, in turn, the positive and negative ions.

4 Modeling Glow Discharge

Ultimately, our goal is to evaluate the point-wise emission term $L_e(\boldsymbol{x},\boldsymbol{\omega})$, from Equation 4, without precomputation. To this end, we avoid global solve approaches, such as FEM, which discretize their domain. These approaches are limited by this discretization process, both in the time required for it and its resulting accuracy. Moreover, it becomes difficult to efficiently adapt these methods for dynamic scenes where boundary conditions change over time. While Monte Carlo PDE approaches [Sawhney and Crane 2020; Sawhney et al. 2022] have found success in overcoming these issues, they are limited to a class of equations that do not entirely encompass Equations 3 (see Section 1 of the supplementary). The apparent deadlock between our goals for interactive rendering and physical accuracy poses a significant challenge. Our solution leans towards the former, and it is achieved by making a series of simplifications in the derivation of our model that enables a more straightforward numerical approach to solving for the particle densities.

In this section, we present a numerical algorithm for obtaining the number densities for each particle. Beginning in Section 4.1, we formulate the evolution of particle densities along their respective

drift velocities. Next, we propose a simplification to align these drift velocities, which makes these equations simpler to solve at any point in the domain. Section 4.3 discusses the boundary conditions of our problem and provides a concrete formula for the particle densities. Finally, Section 4.4 describes a reparameterization of the equations for numerical stability and details the complete algorithm.

4.1 Drift-Aligned Formulation

We shall present the derivation in a top-down approach, beginning with Equations 3. Our model aims to aggregate the time-varying fluctuations in glow discharge. To achieve this, we first assume that the system is in equilibrium, such that $\frac{\partial X}{\partial t} = 0$ for all densities. Additionally, to obtain an efficient local solver, we ignore the diffusion term in Equations 3a, i.e. we assume $\mathcal{D} = 0$.

With these modifications, Equations 3 become the following:

$$0 = \alpha\|\vec{v}_E\|E - \eta\|\vec{v}_E\|E - \beta EP - \nabla\cdot(E\vec{v}_E) \tag{5a}$$
$$0 = \alpha\|\vec{v}_E\|E - \beta EP - \beta NP - \nabla\cdot(P\vec{v}_P) \tag{5b}$$
$$0 = \eta\|\vec{v}_E\|E - \beta NP - \nabla\cdot(N\vec{v}_N) \tag{5c}$$

We can rewrite these equations to express the gradient of the number densities along their drift velocities by expanding and rearranging the divergence term of the right-hand sides, for example:

$$0 = X - \nabla\cdot(E\vec{v}_E) \quad \text{becomes} \quad \nabla_{\vec{v}_E}E = X - (\nabla\cdot\vec{v}_E)E \tag{6}$$

Altogether, the drift-aligned evolution of the densities is summarized below:

$$\nabla_{\vec{v}_E}E = \alpha\|\vec{v}_E\|E - \eta\|\vec{v}_E\|E - \beta EP - (\nabla\cdot\vec{v}_E)E \tag{7a}$$
$$\nabla_{\vec{v}_P}P = \alpha\|\vec{v}_E\|E - \beta EP - \beta NP - (\nabla\cdot\vec{v}_P)P \tag{7b}$$
$$\nabla_{\vec{v}_N}N = \eta\|\vec{v}_E\|E - \beta NP - (\nabla\cdot\vec{v}_N)N \tag{7c}$$

Along the integral curves of each particle's drift velocities, these partial differential equations (PDE) reduce to a system of ordinary differential equations (ODE).

4.2 Homogenizing Drift Velocities

Individually, the ODEs in Equations 7 are simpler to manage than the PDEs in Equations 3, but altogether they are still challenging to solve locally because the drift velocities may be distinct. Our next step involves rewriting each equation using gradients along the same, i.e. homogenized, drift velocity $\vec{\mu}$. Specifically, we let $\vec{v}_E = \vec{\mu}$ as a baseline and define $\vec{v}_P = \vec{v}_N = \rho\vec{\mu}$, where $\rho > 1$ is a constant scalar parameter[1]. This leaves Equation 7a virtually unchanged, but yields useful forms for other equations; for positive ions, we find:

$$\begin{aligned}\nabla_{\rho\vec{\mu}}P &= \alpha\|\vec{\mu}\|E - \beta EP - \beta NP - (\nabla\cdot\rho\vec{\mu})P\\ \nabla_{\vec{\mu}}P &= \tfrac{\alpha}{\rho}\|\vec{\mu}\|E - \tfrac{\beta}{\rho}EP - \tfrac{\beta}{\rho}NP - \tfrac{1}{\rho}(\nabla\cdot\rho\vec{\mu})P\\ \nabla_{\vec{\mu}}P &= \tfrac{\alpha}{\rho}\|\vec{\mu}\|E - \tfrac{\beta}{\rho}EP - \tfrac{\beta}{\rho}NP - (\nabla\cdot\vec{\mu})P\end{aligned} \tag{8}$$

Equation 7c is modified similarly. Ultimately, our homogenized drift-aligned equations of evolution for the number densities are as follows:

$$\nabla_{\vec{\mu}}E = (\alpha-\eta)\|\vec{\mu}\|E - \beta EP - (\nabla\cdot\vec{\mu})E \tag{9a}$$
$$\nabla_{\vec{\mu}}P = \tfrac{\alpha}{\rho}\|\vec{\mu}\|E - \tfrac{\beta}{\rho}EP - \tfrac{\beta}{\rho}NP - (\nabla\cdot\vec{\mu})P \tag{9b}$$
$$\nabla_{\vec{\mu}}N = \tfrac{\eta}{\rho}\|\vec{\mu}\|E - \tfrac{\beta}{\rho}NP - (\nabla\cdot\vec{\mu})N \tag{9c}$$

We assume that $\vec{\mu}$ is approximately a potential flow so that it exhibits no bifurcations. This makes our numerical implementation straightforward, and it is a reasonable assumption since the electric field along which the particles flow is itself a potential flow, i.e. $\vec{E} = \nabla\Phi$, where Φ is the electric potential.

Ideally, $\vec{\mu}$ is computed based on the ambient electric field generated by a specified charge distribution, e.g., on a conductor's surface. However, this would require calculating the computationally costly Coloumb forces at $\boldsymbol{x}$ to evaluate $\vec{\mu}$. Therefore, we choose to manually prescribe $\vec{\mu}$ in a bounded domain. Section 5.3 describes our approach to this, which makes our model amenable to artistic design.

4.3 Point-Wise Derivation

Next, we discuss our methodology for solving for the particle densities at arbitrary points $\boldsymbol{x}$ according to Equations 9. Our configuration involves a bounded domain Ω; we refer to the portion of its interior where $\|\vec{\mu}\| > 0$ (equivalently $\operatorname{Int}\Omega \cap \operatorname{supp}\vec{\mu}$) as the *active region* for the glow discharge. On the boundary, we enforce the following inflow boundary conditions:

$$E = P = N = 1 \quad \text{on} \quad \Gamma = \{\boldsymbol{x} \in \partial\Omega \mid \vec{\mu}(\boldsymbol{x})\cdot\hat{n} < 0\} \tag{10}$$

Define the map $\gamma(\boldsymbol{x}, t)$ which flows $\boldsymbol{x}$ along $\vec{\mu}$ for some time t that is possibly negative. The boundary point corresponding to $\boldsymbol{x}$ is then formalized as $\boldsymbol{x}_\partial = \gamma(\boldsymbol{x}, -\tau)$, where:

$$\tau = \inf_{t\geq 0}\{\gamma(\boldsymbol{x}, -t) \in \partial\Omega\} \tag{11}$$

The inset below illustrates this process.

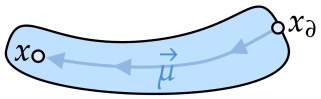

Then, the solution to the number densities at $\boldsymbol{x}$ can be found by integrating over time. As an example, for the electron number density, this becomes:

$$E(\boldsymbol{x}) = \int_{-\tau}^{0}(\alpha-\eta)\|\vec{\mu}_t\|E_t - \beta E_t P_t - (\nabla\cdot\vec{\mu}_t)E_t\,dt \tag{12}$$

Above, we use $\mathcal{X}_t = \mathcal{X}\circ\gamma(\boldsymbol{x}, t)$ for brevity. Algorithmically, our procedure for solving for these densities is as follows: (1) walk backwards along the flow map until $\boldsymbol{x}_\partial$ is reached, then (2) walk forwards for τ units while numerically integrating the densities E, P, and N as in Equation 12.

4.4 Numerical Solver

[1] In glow discharge, the mean free path of all particles is relatively short because of the high densities that arise from electron avalanches. Compared to ions, which have greater mass, electrons are more likely to deviate from their path. For this reason, we prefer to let ρ greater than one.

Typically, glow discharges consist of several millions of particles. To avoid instabilities with large numbers in a numerical implementation we reparameterize the number densities using a logarithmic representation $\mathcal{X} = \exp\widetilde{\mathcal{X}}$. This results in a significant transformation of Equations 9 which, for electron densities, resolves as follows:

$$\begin{aligned} \nabla_{\vec{\mu}} E &= (\alpha-\eta)\|\vec{\mu}\|E - \beta EP - (\nabla\cdot\vec{\mu})E \\ \nabla_{\vec{\mu}}\widetilde{E}\cdot\exp\widetilde{E} &= (\alpha-\eta)\|\vec{\mu}\|\exp\widetilde{E} - \beta\exp(\widetilde{E}+\widetilde{P}) - (\nabla\cdot\vec{\mu})\exp\widetilde{E} \\ \nabla_{\vec{\mu}}\widetilde{E} &= (\alpha-\eta)\|\vec{\mu}\| - \beta\exp\widetilde{P} - (\nabla\cdot\vec{\mu}) \end{aligned} \tag{13}$$

The complete set of reparameterized and homogenized drift-aligned equations for our numerical solvers is shown below:

$$\nabla_{\vec{\mu}}\widetilde{E} = (\alpha-\eta)\|\vec{\mu}\| - \beta\exp\widetilde{P} - (\nabla\cdot\vec{\mu}) \tag{14a}$$

$$\nabla_{\vec{\mu}}\widetilde{P} = \frac{\alpha}{\rho}\|\vec{\mu}\|\exp(\widetilde{E}-\widetilde{P}) - \frac{\beta}{\rho}\exp\widetilde{E} - \frac{\beta}{\rho}\exp\widetilde{N} - (\nabla\cdot\vec{\mu}) \tag{14b}$$

$$\nabla_{\vec{\mu}}\widetilde{N} = \frac{\eta}{\rho}\|\vec{\mu}\|\exp(\widetilde{E}-\widetilde{N}) - \frac{\beta}{\rho}\exp\widetilde{P} - (\nabla\cdot\vec{\mu}) \tag{14c}$$

We put this together with earlier parts of this section in Algorithm 1. The *TraceBackwards* method in lines 1-9 determines the time τ and position $\boldsymbol{x}_\partial$ at the boundary. It is possible that the boundary is not reached within the fixed number of integration steps. In this case, we treat the terminal position as the boundary point, which can lead to bias. We use adaptive time-stepping, through the *AdaptiveRatio* method, to minimize this situation. Once we have the boundary time and position, we integrate particle densities in *IntegrateDensities*, see lines 10-20. Note that for these logarithmic densities, the inflow boundary conditions enforce $\widetilde{\mathcal{X}} = 1$ on Γ. Altogether, these steps are combined in lines 21-24 in *EstimateDensities*. We use different time steps for *TraceBackwards* and *IntegrateDensities* to decouple their computation time. Note that, while we use forward Euler integration, any first-order integration method can be used in place, see Section 4 of the supplementary.

In summary, we have proposed a series of simplifications to Equations 3 that reduce the original PDEs into a set of drift-aligned ODEs that are simpler to solve numerically. As a result, we can query the number densities of electrons at a given point $\boldsymbol{x}$. This becomes necessary to evaluate the volume emission term $L_e(\boldsymbol{x}, \boldsymbol{\omega}, \lambda)$ as highlighted in Equation 4. The next section discusses how we concretely evaluate this emission term on a per-wavelength basis to complete our volume rendering formulation.

Algorithm 1: Numerical solver for number densities.

```
// Evaluate the time |τ| to the boundary
1  Function TraceBackwards(x, Δt, n):
2      p, τ ← (x, 0)
3      for i ← 1 to n do
           // Terminate upon first contact
4          if p ∈ ∂Ω then
5              break
           // Optionally perform adaptive time steps
6          r ← AdaptiveRatio(p)
7          p ← p − μ⃗(p) · rΔt
8          τ ← τ + rΔt
9      return p, τ
   // Solve for particle densities along γ_x(t) (Equation 12)
10 Function IntegrateDdensities(x, Δt, n):
11     p, Ẽ, P̃, Ñ ← (x, 0, 0, 0)
12     for i ← 1 to n do
13         ℓ ← ‖μ⃗(p)‖
14         d ← (∇ · μ⃗)(p)
           // Compute density differentials (Equations 14)
15         ΔẼ ← (α − η)ℓ − β exp P̃ − d
16         ΔP̃ ← (αℓ/ρ) exp(Ẽ − P̃) − (β/ρ) exp Ẽ − (β/ρ) exp P̃ − d
17         ΔÑ ← (ηℓ/ρ) exp(Ẽ − Ñ) − (β/ρ) exp P̃ − d
           // Forward Euler integration step
18         X̃ ← X̃ + ΔX̃ · Δt
19         p ← p + Δt μ⃗(p)
20     return Ẽ, P̃, Ñ
21 Function EstimateDensities(x, Δt, N1, N2):
22     p, τ ← TraceBackwards(x, Δt, N1)
23     Ẽ, P̃, Ñ ← IntegrateDensities(p, τ/N2, N2)
24     return Ẽ, P̃, Ñ
```

5 Volume Rendering

Given the number density of the electrons at a given location, we can use Equation 4 to model the outgoing emission at that point. Section 5.1 describes how to obtain the per-wavelength emissions at any point based on the spectroscopic properties of the gas. Finally, in Section 5.2, we discuss how to perform volume rendering of glow discharge with Monte Carlo integration.

5.1 Spectrosopic Emission

We must convert the number densities $\mathcal{X}$ into radiance used during volume rendering. We model the spectroscopic emissions from glow discharge similarly to Pegoraro and Parker [2006]. The implication of Equation 4 is that the per-wavelength radiance from $\boldsymbol{x}$ along $\boldsymbol{\omega}$ is

Wavelength Emission

$$L_e(\boldsymbol{x}, \boldsymbol{\omega}, \lambda) = \left(\frac{P_\lambda \sigma_0}{4\pi}\right)\|\vec{\mu}\|E(\boldsymbol{x}) \tag{15}$$

where P_λ measures the probability that emitted photons have wavelength λ. Within the visible spectrum, only a few wavelengths are emitted from de-excitation. These correspond to electronic[2] energy state transitions from a higher energy state $\mathcal{E}_h$ to $\mathcal{E}_l$ which, by Planck's law, emit photons of wavelength $\lambda = \frac{hc}{\mathcal{E}_h - \mathcal{E}_l}$ where h is Planck's constant and c is the speed of light. The frequency of these transitions is given by the Einstein coefficient A_{hl} of spontaneous emission. Altogether, we model the probability P_λ using a

[2] As opposed to rotational and vibrational transitions prevalent in molecules.

temperature-dependent Maxwell-Boltzmann distribution:

Probability	Weighted Sum
$P_\lambda = \frac{g_h A_{hl}}{Z} \exp\left(-\frac{\mathcal{E}_h}{k_B T}\right)$	$Z = \sum_i g_i A_{ij} \exp\left(-\frac{\mathcal{E}_i}{k_B T}\right)$

(16)

Here, k_B is the Boltzmann constant, g_i is the degeneracy of the i^{th} energy state, and j is the index of the lower energy state for each i. The temperature T can be approximated by the thermal velocity of the electrons in the system, $T = \frac{m_e}{k_B} \|\vec{\mu}\|^2$. In practice, we rely on tabulated values $A_{ij}, \mathcal{E}$, and g of the transitions, found in chemical databases such as NIST [Ralchenko 2005] and HITRAN [Rothman et al. 2009]. Figure 3 shows our results.

Fig. 3. **Spectroscopic emission.** Our model accounts for the spectroscopic emissions of the particular gas medium. We can therefore simulate lighting from distinct lights characterized by the elemental gas. This is demonstrated above, where each letter and symbol is composed of a different gas. The gases used are Sodium, Hydrogen, Helium, Mercury, Krypton, Nitrogen, Neon, Argon, and Xenon.

5.2 Monte Carlo Estimator

To use the emission term from Equation 15, we perform integration along rays as indicated in Equation 2. The one-dimensional integral can be estimated using Monte Carlo integration with uniform samples taken along the ray [Novák et al. 2018]. Our implementation uses a one-sample estimator, $\langle L_o \rangle = d \cdot L_e(\boldsymbol{x}_0 + \xi \cdot d\boldsymbol{\omega}, \lambda)$, where ξ is sampled from $U(0, 1)$.

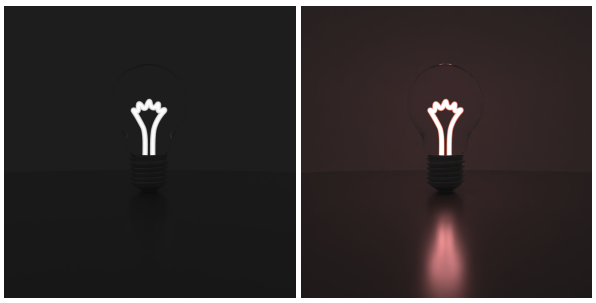

Fig. 4. **Volume rendering.** We render our glow discharge model using volume rendering. An instance of glow discharge (right, reddish), characterized by its active region (left, white), participates in standard light transport effects. In the example above, we demonstrate effects including refraction from the glass bulb and glossy reflections on the floor. Scene adapted from Incandescent Glass Light Bulb by Leo Blanchette ©TurboSquid.

In a practical rendering system, we bound the active region of the glow discharge, for example by using a bounding box, and evaluate the estimator only within this volume. If a ray intersects a surface that is partially contained within the bounding volume, the next scattering event is forwarded to that surface. This design allows our glow discharge model to integrate seamlessly with other types of primitives and to participate naturally in global light transport effects. We demonstrate this in Figure 4, where emission from the glow discharge interacts with glass and glossy surfaces. A gallery of scenes with involving various light transport effects is displayed in Figure 7.

5.3 Modeling Drift Velocities

The previous sections detailed the derivation and application of a model for glow discharge for volume rendering. Our model consists of multiple scalar parameters that can alter the local emissive intensity (see Section 6.2); however these alone cannot change the broader shape of the glow discharge. The primary role of the homogenized drift velocity $\vec{\mu}$ is therefore to shape the glow discharge by prescribing local particle velocities.

The velocity field $\vec{\mu}$ can be assigned arbitrarily as long as it is continuous and approximately a potential flow (recall Section 4.2). To ease the design of this field, our implementation relies on quadratic Bezier curves[3] as primitives for describing $\vec{\mu}$. The active region corresponding to a collection of Bezier curves is a capsule of fixed radius r. For any point $\boldsymbol{x}$ in this region, we can associate a closest point $\boldsymbol{c}$ to the curves, curve time t, and cross-sectional angle θ. Using this data, we can define *laminar* and *extruding* flows as follows

Laminar Flow	Extruding Flow
$\vec{\mu}(\boldsymbol{x}) = f(t, \theta) \cdot \mathcal{T}(t)$	$\vec{\mu}(\boldsymbol{x}) = f(t, \theta) \cdot \mathcal{N}(t)$

(17)

where $\mathcal{T}(t) = Q'(t)$ is the curve tangent, $\mathcal{N}(t)$ is the curve normal facing $\boldsymbol{c}$, and $f(t, \theta)$ is an arbitrary modulator. In practice, we use a collection of Bezier curves confined to a bounding volume, in which case the signed distance and closest point queries must account for all curves.

6 Results

We now present the results of our glow discharge model. In Section 6.2, we demonstrate the effects of the various scalar parameters of our model and additionally provide intuition for what each controls. Comparisons with realistic instances of glow discharge are shown in Section 6.3. We briefly discuss the performance and computational overhead of using our model in Section 6.4.

6.1 Implementation

Our method is built on top of a volumetric path tracer which uses BRDF sampling only. All images presented in this work are rendered with 1024 samples and are subsequently denoised using Intel Open Image Denoise [Áfra 2025], see Section 3 of the supplementary for details. The path tracer is implemented using the Vulkan graphics

[3]We avoid cubic Bezier curves as solving for the signed distance is costlier and less accurate than for quadratic Bezier curves.

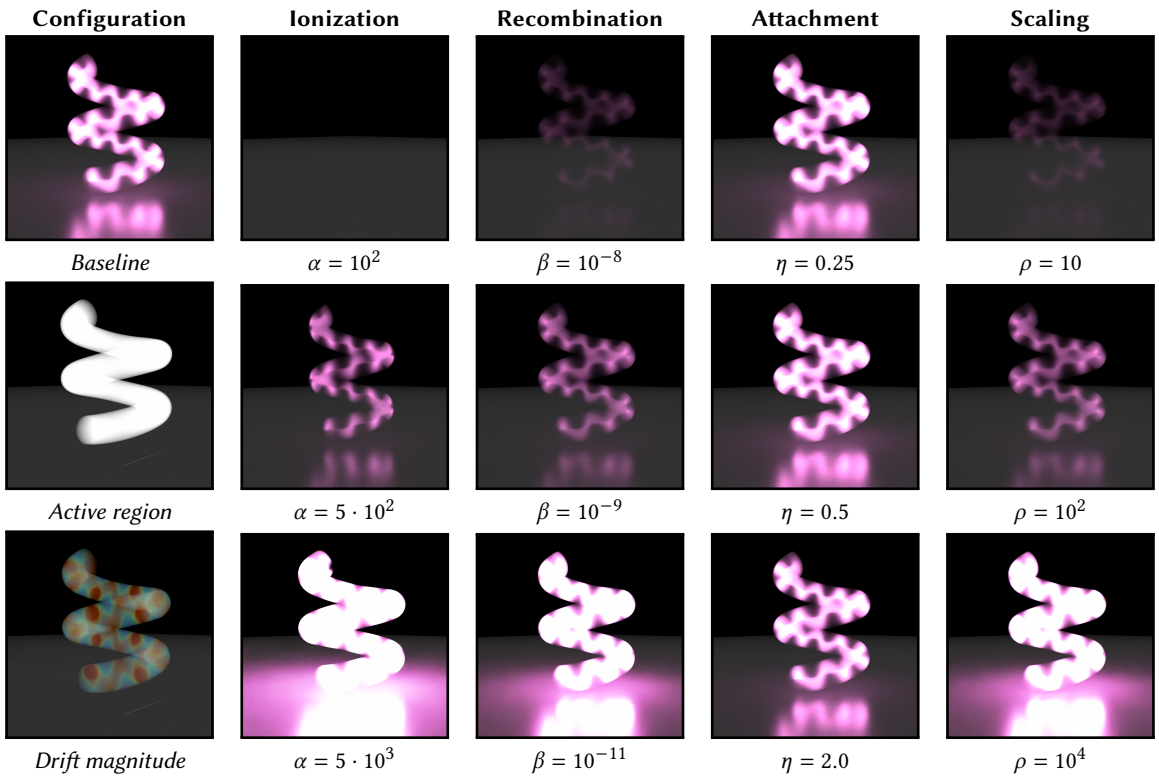

Fig. 5. **Model parameters.** Above, we show the effect of tuning the various parameters of our model. In the left column, we show the baseline configuration, its active region, and the magnitude of the drift velocity (blue is lower, red is higher). Generally, the highest impact on the emission's strength is due to the ionization, recombination, and scaling coefficients. As ionization and scaling increases, one can expect brighter discharges; increasing the recombination coefficient reduces the amount of emission.

API, with raytracing support, and runs on an NVIDIA 4090 RTX graphics processing unit.

6.2 Model Parameters

In Figure 5, we compare the effects of each scalar parameter in our model. The baseline rendering uses parameters $(\alpha, \beta, \eta, \rho) = (10^3, 10^{-10}, 1, 10^3)$ for the medium, and $N_1 = N_2 = 1024$ for the numerical solver in Algorithm 1. For the drift velocity, we apply an extruding flow along a small set of Bézier curves forming a helix, with velocity modulated along the cross-sectional angle θ. Below, we describe the qualitative impact of each parameter.

Ionization (α). The ionization coefficient directly controls the intensity of the resulting emissions, which is consistent with the emission formulation in Equation 15. If the ionization coefficient is too low, the electrons generated through ionization are quickly consumed through recombination or attachment, resulting in little to no emission.

Recombination (β). The recombination coefficient acts as a drag term on the exponential growth of the electron number density. Increasing the recombination coefficient reduces the resulting emissions, while reducing it allows for higher electron densities and brighter discharges.

Attachment (η). The attachment coefficient, like the recombination coefficient, reduces the growth of positive ions by recombination and restores the growth of electrons. However, it also suppresses the growth of electrons through attachment. In practice, its effect on the visual qualities of the discharge is negligible.

Scaling (ρ). Increasing the scaling coefficient slows the growth of both positive and negative ions. As a result, larger emission intensities are observed. We note that increasing the scaling coefficient produces similar effects to reducing the recombination coefficient, suggesting potential redundancy between the two.

When comparing the impact on emission intensity, the ionization, recombination, and scaling coefficients are the most significant.

6.3 Real World Comparisons

Our model is capable of replicating real-world instances of glow discharge. In Figure 6, we reproduce an example of corona discharge, where high voltage applied to a metal spoon causes filaments of glow discharge to form at various points on its surface. To mimic this, we procedurally generate a collection of glow discharge primitives (i.e. Bézier curves), as described in Section 2 of the supplementary material. Qualitatively, our synthesized scene captures the visual characteristics of the individual filaments observed in the reference.

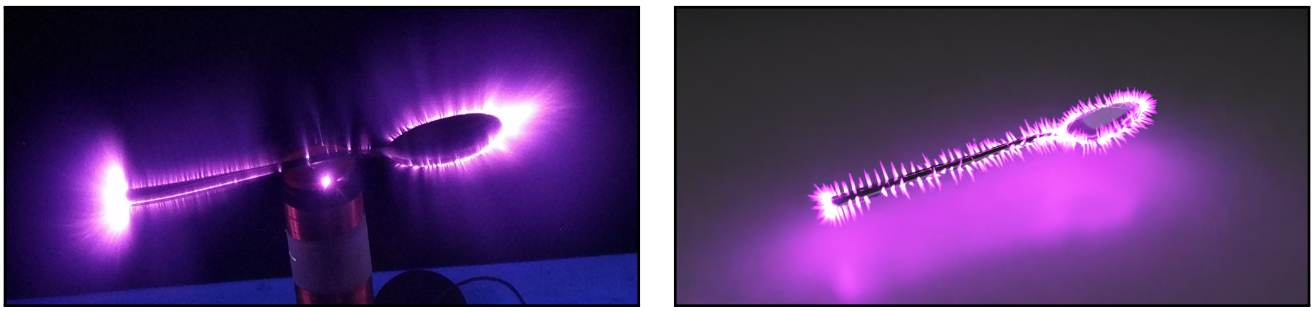

Fig. 6. **Real world comparison.** We compare our glow discharge model to the real world by replicating the strands that appear due to Corona discharge (left). Each strand in our version (right) is a curve primitive whose drift velocity decreases along its length. Our model can roughly match the colors observed in the real world in these kinds of phenomena. The ambient gas is Nitrogen (N_2), which air primarily consists of, hence the purple glow. Scene adapted from Cutlery set 02 by the_nikiforov ©TurboSquid.

Car Horse Tunnel

Fig. 7. **Gallery of results.** Our glow discharge lighting model can be used instead of traditional light sources to provide the full lighting for a scene. Above, we demonstrate scenes that are lit exclusively through glow discharge primitives. Car is adapted from Chrysler Saratoga 1960 by tedpermana ©TurboSquid; Horse uses the model Horse Statue 01 by Rico Cilliers ©Poly Haven; Tunnel modifies Sci Fi Tunnel by Emscgi ©TurboSquid.

Each strand appears brightest (white) near the spoon and transitions to purple as it extends outward, consistent with the behavior of corona discharge filaments in the real-world example. Figures 1 and 7 shows our renderings when applied to various kinds of scenes.

6.4 Solver Evaluation

We now evaluate the numerical solver detailed in Algorithm 1. Our model aims to be both physically-based *and* practical for interactive rendering.

Comparison to FEM. Discarding the diffusion term by setting $\mathcal{D} = 0$ in Equations 5 constitutes a significant simplification. We evaluate its impact in Figure 8 by comparing our solver to a FEM baseline. When the diffusion coefficient is small, i.e., $\mathcal{D} \leq 10^{-4}$, our solver produces solutions that are visually comparable to those from FEM. However, increasing $\mathcal{D}$ beyond a threshold such as 10^{-2} results in noticeable divergence between the two.

Tuning solver iterations. Algorithm 1 includes tunable iteration parameters, N_1 and N_2. The parameter N_1 sets the maximum number of allowed iterations for reaching the boundary during the backward tracing phase, while N_2 controls the time resolution used for integrating the final densities. Figure 9 shows the effects of halving each parameter independently and jointly. The results indicate that reducing N_1 has a more pronounced effect on the solution than reducing N_2.

Performance evaluation. Table 2 lists the frametimes for each of the scenes presented in this paper. In general, our solver maintains interactive performance, and lowering the iteration parameters leads to improved frametimes.

7 Conclusion

In this work, we present a physically-based approach for simulating and rendering glow discharge. We derive a model to estimate particle number densities and use this to compute pointwise emissions, integrating seamlessly with existing volume rendering architectures. Our method offers a practical way to simulate realistic light sources shaped by charged particle dynamics.

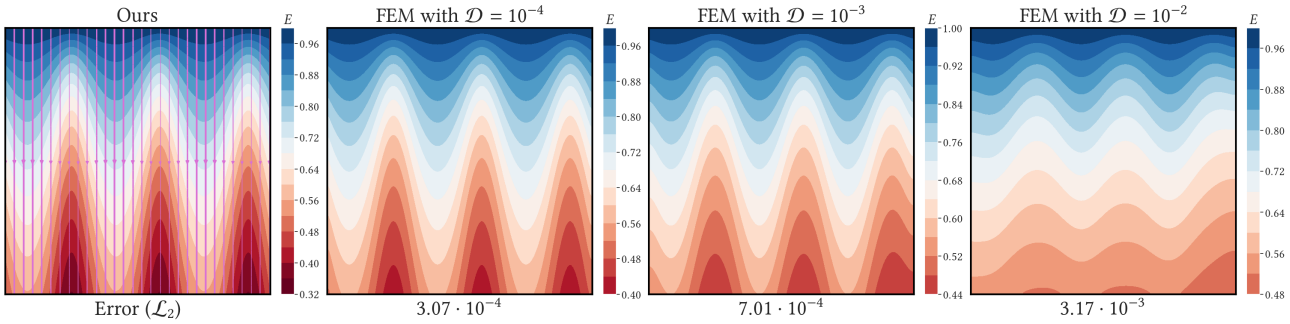

Fig. 8. **Comparison to FEM.** The insets above compare an FEM solver with our numerical integrator under varying magnitudes of the diffusion coefficient. When the diffusion coefficient is small, the results are comparable. As diffusion becomes more significant, the FEM solution diverges from ours. All other coefficients are held constant at $(\alpha, \beta, \eta, \rho) = (1, 1, 1, 1)$.

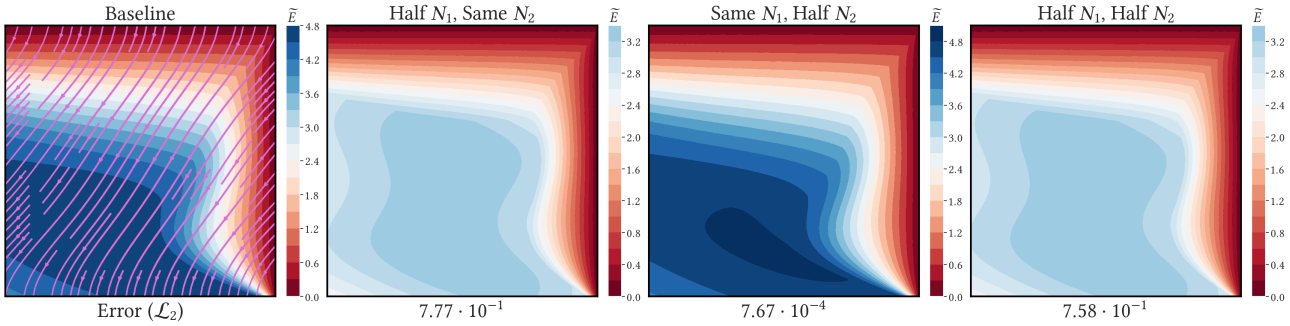

Fig. 9. **Tweaking solver iterations.** Modifying the number of iterations in our numerical solver (Algorithm 1) can alter the evaluated densities. Above, we demonstrate the differences resulting from halving N_1 and N_2, which are 512 and 32 in the baseline, respectively. The discrepancy in results is significantly larger when halving N_1, highlighting the solver's reliance on the backward tracing phase. The coefficients used in this example are $(\alpha, \beta, \eta, \rho) = (10, 1, 1, 10)$.

Table 2. **Solver performance.** The tables below list the frametimes of our path tracer for various scenes (left) and iteration configurations (right).

Scene	Curves	Time (ms)	N_1	N_2	Time (ms)
Car	188	195	1024	1024	110
Horse	224	139	1024	512	83
Siggraph	236	230	1024	256	69
Tunnel	504	110	512	1024	90
Spoon	1024	1166	256	1024	78
Chess	1216	200	512	512	58

Limitations and future work. Our model introduces simplifications that, while aiding tractability, may obscure the physical meaning of certain parameters. For example, empirical measurements–such as ionization rates–do not directly map to coefficients in our formulation. Moreover, our volumetric path tracer currently relies on BRDF sampling; incorporating next-event estimation and advanced light sampling heuristics derived from our model could improve rendering efficiency and accuracy. A natural extension of this work is to simulate spark discharges such as lightning, which occur on larger spatial and temporal scales and exhibit more complex dynamics.

Scientific applications. Glow discharge plays a role in many engineering and industrial systems. In Direct Current sputtering, used for thin-film deposition, controlling the plasma's shape and stability is critical for producing uniform coatings. In high-voltage power transmission, a related phenomenon–corona discharge–leads to ionization of surrounding air, causing energy loss and interference. Our model offers a fast, approximate solver for glow discharge behavior, making it suitable for applications such as previsualization tools. Users could, for instance, specify expected drift velocities and observe the resulting charged particle distributions.

8 Acknowledgements

This work was funded in part by the Ronald L. Graham Chair and the UC San Diego Center for Visual Computing. We also acknowledge NSF grants 2238839 and 2402583, and gifts from Adobe, Google, Qualcomm and Rembrand.

References

Attila T. Áfra. 2025. Intel® Open Image Denoise. https://www.openimagedenoise.org.
Peter Atkins and Julio De Paula. 2006. *Physical chemistry.* Vol. 1. Macmillan.
Mégane Bati, Stéphane Blanco, Christophe Coustet, Vincent Eymet, Vincent Forest, Richard Fournier, Jacques Gautrais, Nicolas Mellado, Mathias Paulin, and Benjamin Piaud. 2023. Coupling Conduction, Convection and Radiative Transfer in a Single Path-Space: Application to Infrared Rendering. *ACM Trans. Graph.* 42, 4, Article 79 (July 2023), 20 pages. https://doi.org/10.1145/3592121

Djilali Benyoucef and Toufik Tahri. 2017. Air molecule collision cross sections: calculation and validation. *Canadian Journal of Physics* 95, 4 (2017), 346–352. https://doi.org/10.1139/cjp-2016-0406

Hans Dieter Betz, Ulrich Schumann, and Pierre Laroche. 2008. Lightning: principles, instruments and applications: review of modern lightning research. (2008).

Subrahmanyan Chandrasekhar. 1960. *Radiative transfer*. Dover Corporation.

Vernon Cooray. 2015. *An introduction to lightning*. Vol. 201. Springer.

Ivan T. Cruz, Marcelo M. F. Saba, José Claudio O. Silva, Rasha U. Abbasi, Hugh G. P. Hunt, Carina Schumann, Diego R. R. da Silva, Tagianne P. da Silva, Paola B. Lauria, and Ny T. Kieu. 2025. Correlation Between Speed of the Leader and Peak Current of the Return Stroke in Negative Lightning Flashes. *Geophysical Research Letters* 52, 2 (2025), e2024GL111594. https://doi.org/10.1029/2024GL111594 arXiv:https://agupubs.onlinelibrary.wiley.com/doi/pdf/10.1029/2024GL111594 e2024GL111594 2024GL111594.

A Dalgarno. 2006. The galactic cosmic ray ionization rate. *Proceedings of the National Academy of Sciences* 103, 33 (2006), 12269–12273.

Joseph R Dwyer and Martin A Uman. 2014. The physics of lightning. *Physics Reports* 534, 4 (2014), 147–241.

S Flugge. 1955. *Electron Emission Gas Discharges I.* Springer.

G E Georghiou, R Morrow, and A C Metaxas. 2000. Two-dimensional simulation of streamers using the FE-FCT algorithm. *Journal of Physics D: Applied Physics* 33, 3 (feb 2000), L27. https://doi.org/10.1088/0022-3727/33/3/101

James W Gewartowski and Hugh A Watson. 1965. Principles of electron tubes: including grid-controlled tubes, microwave tubes, and gas tubes. *(No Title)* (1965).

Wojciech Jarosz, Matthias Zwicker, and Henrik Wann Jensen. 2008. The beam radiance estimate for volumetric photon mapping. In *ACM SIGGRAPH 2008 Classes* (Los Angeles, California) *(SIGGRAPH '08)*. Association for Computing Machinery, New York, NY, USA, Article 3, 112 pages. https://doi.org/10.1145/1401132.1401137

Xuechen Li, Panpan Zhang, Pengying Jia, Jingdi Chu, and Junying Chen. 2017. Generation of a planar direct-current glow discharge in atmospheric pressure air using rod array electrode. *Scientific Reports* 7, 1 (2017), 2672.

Wayne M Lowder and Harold L Beck. 1966. Cosmic-ray ionization in the lower atmosphere. *Journal of Geophysical Research* 71, 19 (1966), 4661–4668.

Alejandro Malagón-Romero and Alejandro Luque. 2019. Spontaneous emergence of space stems ahead of negative leaders in lightning and long sparks. *Geophysical Research Letters* 46, 7 (2019), 4029–4038.

Françoise Massines, Ahmed Rabehi, Philippe Decomps, Rami Ben Gadri, Pierre Ségur, and Christian Mayoux. 1998. Experimental and theoretical study of a glow discharge at atmospheric pressure controlled by dielectric barrier. *Journal of Applied Physics* 83, 6 (03 1998), 2950–2957. https://doi.org/10.1063/1.367051

Bailey Miller, Iliyan Georgiev, and Wojciech Jarosz. 2019. A null-scattering path integral formulation of light transport. *ACM Transactions on Graphics (Proceedings of SIGGRAPH)* 38, 4 (July 2019). https://doi.org/10/gf6rzb

Bailey Miller, Rohan Sawhney, Keenan Crane, and Ioannis Gkioulekas. 2023. Boundary Value Caching for Walk on Spheres. *ACM Trans. Graph.* 42, 4 (2023).

Bailey Miller, Rohan Sawhney, Keenan Crane, and Ioannis Gkioulekas. 2024a. Walkin' Robin: Walk on Stars with Robin Boundary Conditions. *ACM Trans. Graph.* 43, 4 (2024).

Bailey Miller, Rohan Sawhney, Keenan Crane, and Ioannis Gkioulekas. 2024b. Walkin' Robin: Walk on Stars with Robin Boundary Conditions. *ACM Trans. Graph.* 43, 4, Article 41 (July 2024), 18 pages. https://doi.org/10.1145/3658153

R. Morrow. 1985. Theory of negative corona in oxygen. *Phys. Rev. A* 32 (Sep 1985), 1799–1809. Issue 3. https://doi.org/10.1103/PhysRevA.32.1799

R Morrow and J J Lowke. 1997. Streamer propagation in air. *Journal of Physics D: Applied Physics* 30, 4 (feb 1997), 614. https://doi.org/10.1088/0022-3727/30/4/017

Michael B. Nielsen, Morten Bojsen-Hansen, Konstantinos Stamatelos, and Robert Bridson. 2022. Physics-Based Combustion Simulation. *ACM Trans. Graph.* 41, 5, Article 176 (May 2022), 21 pages. https://doi.org/10.1145/3526213

Jan Novák, Iliyan Georgiev, Johannes Hanika, Jaroslav Křivánek, and Wojciech Jarosz. 2018. Monte Carlo Methods for Physically Based Volume Rendering. In *ACM SIGGRAPH 2018 Courses* (Vancouver, British Columbia, Canada) *(SIGGRAPH '18)*. ACM, New York, NY, USA, Article 14, 1 pages. https://doi.org/10.1145/3214834.3214880

Jan Novák, Derek Nowrouzezahrai, Carsten Dachsbacher, and Wojciech Jarosz. 2012. Virtual ray lights for rendering scenes with participating media. *ACM Trans. Graph.* 31, 4, Article 60 (July 2012), 11 pages. https://doi.org/10.1145/2185520.2185556

Vincent Pegoraro and Steven G. Parker. 2006. Physically-based realistic fire rendering. In *Proceedings of the Second Eurographics Conference on Natural Phenomena (NPH'06)*. Eurographics Association, 51–59.

Matt Pharr, Wenzel Jakob, and Greg Humphreys. 2016. *Physically Based Rendering: From Theory to Implementation* (3rd ed.). Morgan Kaufmann, Cambridge, MA. https://www.pbrt.org/

Yuri Ralchenko. 2005. NIST atomic spectra database. *Memorie della Società Astronomica Italiana Supplement, v. 8, p. 96 (2005)* 8 (2005), 96.

Todd Reed and Brian Wyvill. 1994. Visual simulation of lightning. In *Proceedings of the 21st Annual Conference on Computer Graphics and Interactive Techniques (SIGGRAPH '94)*. Association for Computing Machinery, New York, NY, USA, 359–364. https://doi.org/10.1145/192161.192256

Jordi-Roger Riba. 2022. Spectrum of Corona Discharges and Electric Arcs in Air under Aeronautical Pressure Conditions. *Aerospace* 9, 9 (2022). https://doi.org/10.3390/aerospace9090524

Damien Rioux-Lavoie, Ryusuke Sugimoto, Tümay Özdemir, Naoharu H. Shimada, Christopher Batty, Derek Nowrouzezahrai, and Toshiya Hachisuka. 2022. A Monte Carlo Method for Fluid Simulation. *ACM Trans. Graph.* 41, 6, Article 240 (Nov. 2022), 16 pages. https://doi.org/10.1145/3550454.3555450

Farouk A. M. Rizk. 2024. Modeling of Lightning Stepped Leader Characteristics. *IEEE Transactions on Dielectrics and Electrical Insulation* 31, 4 (2024), 2055–2063. https://doi.org/10.1109/TDEI.2024.3372485

Laurence S Rothman, Iouli E Gordon, Alain Barbe, D Chris Benner, Peter F Bernath, Manfred Birk, Vincent Boudon, Linda R Brown, Alain Campargue, J-P Champion, et al. 2009. The HITRAN 2008 molecular spectroscopic database. *Journal of Quantitative Spectroscopy and Radiative Transfer* 110, 9-10 (2009), 533–572.

Iman Sadeghi, Adolfo Munoz, Philip Laven, Wojciech Jarosz, Francisco Seron, Diego Gutierrez, and Henrik Wann Jensen. 2012. Physically-based simulation of rainbows. *ACM Trans. Graph.* 31, 1, Article 3 (Feb. 2012), 12 pages. https://doi.org/10.1145/2077341.2077344

Rohan Sawhney and Keenan Crane. 2020. Monte Carlo Geometry Processing: A Grid-Free Approach to PDE-Based Methods on Volumetric Domains. *ACM Trans. Graph.* 39, 4 (2020).

Rohan Sawhney, Daqi Lin, Markus Kettunen, Benedikt Bitterli, Ravi Ramamoorthi, Chris Wyman, and Matt Pharr. 2024. Decorrelating ReSTIR Samplers via MCMC Mutations. *ACM Trans. Graph.* 43, 1, Article 10 (Jan. 2024), 15 pages. https://doi.org/10.1145/3629166

Rohan Sawhney, Bailey Miller, Ioannis Gkioulekas, and Keenan Crane. 2023a. Walk on Stars: A Grid-Free Monte Carlo Method for PDEs with Neumann Boundary Conditions. *ACM Trans. Graph.* 42, 4 (2023).

Rohan Sawhney, Bailey Miller, Ioannis Gkioulekas, and Keenan Crane. 2023b. Walk on Stars: A Grid-Free Monte Carlo Method for PDEs with Neumann Boundary Conditions. *ACM Transactions on Graphics* 42, 4 (July 2023), 1–20. https://doi.org/10.1145/3592398

Rohan Sawhney, Dario Seyb, Wojciech Jarosz, and Keenan Crane. 2022. Grid-Free Monte Carlo for PDEs with Spatially Varying Coefficients. *ACM Trans. Graph.* XX, X (2022).

Florian Simon, Johannes Hanika, Tobias Zirr, and Carsten Dachsbacher. 2017. Line Integration for Rendering Heterogeneous Emissive Volumes. *Computer Graphics Forum (Proceedings of Eurographics Symposium on Rendering)* 36, 4 (2017), 101–110.

Karl Sims. 1990. Particle animation and rendering using data parallel computation. *SIGGRAPH Comput. Graph.* 24, 4 (Sept. 1990), 405–413. https://doi.org/10.1145/97880.97923

Batjargal Sosorbaram, Tadahiro Fujimoto, Kazunobu Muraoka, and Norishige Chiba. 2001. Visual Simulation of Lightning Taking into Account Cloud Growth. In *Proceedings of the International Conference on Computer Graphics (CGI '01)*. IEEE Computer Society, USA, 89.

Ryusuke Sugimoto, Christopher Batty, and Toshiya Hachisuka. 2024. Velocity-Based Monte Carlo Fluids. In *ACM SIGGRAPH 2024 Conference Papers* (Denver, CO, USA) *(SIGGRAPH '24)*. Association for Computing Machinery, New York, NY, USA, Article 8, 11 pages. https://doi.org/10.1145/3641519.3657405

Ryusuke Sugimoto, Terry Chen, Yiti Jiang, Christopher Batty, and Toshiya Hachisuka. 2023. A Practical Walk-on-Boundary Method for Boundary Value Problems. *ACM Trans. Graph.* 42, 4, Article 81 (July 2023), 16 pages. https://doi.org/10.1145/3592109

Nghia Truong, Cem Yuksel, and Larry Seiler. 2020. Quadratic Approximation of Cubic Curves. *Proc. ACM Comput. Graph. Interact. Tech.* 3, 2, Article 16 (Aug. 2020), 17 pages. https://doi.org/10.1145/3406178

Rex West, Iliyan Georgiev, Adrien Gruson, and Toshiya Hachisuka. 2020. Continuous multiple importance sampling. *ACM Trans. Graph.* 39, 4, Article 136 (Aug. 2020), 12 pages. https://doi.org/10.1145/3386569.3392436

Rex West, Iliyan Georgiev, and Toshiya Hachisuka. 2022. Marginal Multiple Importance Sampling. In *SIGGRAPH Asia 2022 Conference Papers* (Daegu, Republic of Korea) *(SA '22)*. Association for Computing Machinery, New York, NY, USA, Article 42, 8 pages. https://doi.org/10.1145/3550469.3555388

Rex West and Sayan Mukherjee. 2024. Stylized Rendering as a Function of Expectation. *ACM Trans. Graph.* 43, 4, Article 96 (July 2024), 19 pages. https://doi.org/10.1145/3658161

Michael R. Winchester and Richard Payling. 2004. Radio-frequency glow discharge spectrometry:: A critical review. *Spectrochimica Acta Part B: Atomic Spectroscopy* 59, 5 (2004), 607–666. https://doi.org/10.1016/j.sab.2004.02.013

Xuxin Yang, Antti Rasila, and Tommi Sottinen. 2017. Walk on spheres algorithm for Helmholtz and Yukawa equations via Duffin correspondence. *Methodology and Computing in Applied Probability* 19 (2017), 589–602.

Shilin Zhu, Xianyao Zhang, Gerhard Röthlin, Marios Papas, and Mark Meyer. 2023. Denoising production volumetric rendering. In *ACM SIGGRAPH 2023 Talks*. 1–2.